Ensemble Solute Transport in 2-D Operator-Scaling Random Fields

Nathan D. Monnig and David A. Benson
Colorado School of Mines, Golden, CO, U.S.A.

Mark M. Meerschaert
Michigan State University, East Lansing, MI, U.S.A.

1. Abstract

Motivated by field measurements of aquifer hydraulic conductivity (K), recent techniques were developed to construct anisotropic fractal random fields, in which the scaling, or self-similarity parameter, varies with direction and is defined by a matrix. Ensemble numerical results are analyzed for solute transport through these 2-D "operator-scaling" fractional Brownian motion (fBm) $\ln(K)$ fields. Both the longitudinal and transverse Hurst coefficients, as well as the "radius of isotropy" are important to both plume growth rates and the timing and duration of breakthrough. It is possible to create osfBm fields that have more "continuity" or stratification in the direction of transport. The effects on a conservative solute plume are continually faster-than-Fickian growth rates, highly non-Gaussian shapes, and a heavier tail early in the breakthrough curve. Contrary to some analytic stochastic theories for monofractal K fields, the plume growth rates never exceed *Mercado's* [1967] purely stratified aquifer growth rate of plume apparent dispersivity proportional to mean distance. Apparent super-stratified growth must be the result of other demonstrable factors, such as initial plume size.

2. Introduction

The first analytical studies of the stochastic ADE used finite correlation length random hydraulic conductivity (K) fields and found that plumes transition from purely stratified growth rates to Fickian growth after traversing a number of correlation lengths [*Gelhar and Axness*, 1983]. Analysis of reported dispersivity versus plume size suggested that real plumes might not reach the Fickian limit [e.g., *Welty and Gelhar* 1989]. Fractional Brownian motion (fBm) was, initially, an attractive model for aquifer hydraulic conductivity because it describes evolving heterogeneity at all scales, typical of many real-world data sets [e.g., *Molz et al.*, 1990]. Furthermore, it could explain continuous super-Fickian plume growth. However, when the power spectrum (Fourier transform of the correlation function) of fBm is used in the classical linearized and small-perturbation solution of the stochastic ADE (see *Neuman*, [1990] and *Di Federico and Neuman* [1998b]), the growth rate not only can be faster than Fickian, but faster than the purely stratified model theorized by *Mercado* [1967]. This faster-than-Mercado result for a plume in a single aquifer has been used to explain the growth of plumes in different aquifers at different scales [*Neuman*, 1990]. However, this finding depends on several assumptions on top of the typical small-perturbation assumptions and has not (to our knowledge) been duplicated in a numerical experiment. *Hassan et al.* [1997] ran numerical transport experiments in low-heterogeneity fractal fields and found, as expected, super-Fickian growth, but the upper limit of the growth rate was not shown. Herein we investigate whether sustained super-Mercado growth rates may be attained by a single or an ensemble plume, and also explore other factors that could contribute to the apparent super-Mercado growth described by *Welty and Gelhar* [1989], *Neuman* [1990], and *Gelhar et al.* [1992].

Most previous fBm models have been defined by a Hurst coefficient H that is independent of direction. *Rajaram and Gelhar* [1995], *Zhan and Wheatcraft* [1996], and *Di Federico et al.* [1999] defined statistically anisotropic fBm in which the strength of the correlation of the increments varied smoothly around the unit circle, but the correlation decay rate versus separation distance falls off with the same power-law in all directions. The order of the power law defines the scaling coefficient H. If this value does not vary with direction in an fBm random field, we refer to it as having isotropic scaling. This isotropic scaling is an unrealistic assumption for granular sedimentary aquifers—it is likely that there is more persistent correlation in the horizontal and/or dip direction compared to the strike or vertical directions. Based on analyses of four hydraulic conductivity sets, *Liu and Molz* [1997a] found that the power-law scaling can vary significantly in the horizontal and vertical directions in agreement with past findings [*Hewett*, 1986; *Molz and Boman*, 1993, 1995]. Among others, *Deshpande et al.* [1997], *Tennekoon et al.* [2003], *Castle et al.* [2004], and *Benson et al.* [2006] also presented evidence of anisotropic scaling in real-world sedimentary rock.

We use a numerical technique [*Benson et al.*, 2006] that can construct random fields with anisotropic scaling. Those authors presented a generalization of classic isotropic fBm called operator-scaling fractional Brownian motion (osfBm) that both allowed for anisotropic scaling as well as varying degrees of directional continuity in the K structure. The "mixing measure" or weight function has the potential to model directionality that may be closely related to depositional patterns. This continuity can be defined by a probability measure on the curve defined by the "radius of isotropy" in 2-D (see Figure 1). The "radius of isotropy" is the radius of an osfBm at which there is no anisotropic rescaling of space (Figure 1). This radius of isotropy is a mathematical parameter of osfBm fields that could potentially be measured from observation of the convolution kernel (Figure 2), which can be directly calculated from the correlation function [*Molz et al.*, 1997]. The radius of isotropy is an important parameter of osfBm fields as it can significantly affect the directional continuity of the fields.

Some difficulties arise when applying a numerical flow model to fractal fields—a true fBm is scale invariant, and has infinite correlation extent. These properties must naturally be violated when simulating fBm numerically on a finite domain, by imposing a high and low-frequency cutoff corresponding to the grid and the domain sizes respectively. *Painter and Mahinthakumar* [1999] and *Herrick et*

0043-1397 /07/$9.00

al. [2002] found that prediction uncertainty is strongly affected by the system size and the propagation of boundary conditions deep into the modeled domain. Both *Ababou and Gelhar* [1990] and *Zhan and Wheatcraft* [1996] argue that the high-frequency (small scale) cutoff is important to transport for small values of the Hurst coefficient. However, according to *Di Federico and Neuman* [1997] the high-frequency cutoff does not significantly influence the properties of fractal fields given sufficient separation between the low and high-frequency cutoffs.

FBm and its extensions are based on convolution of an uncorrelated random Gaussian "noise" with a kernel $\varphi(\boldsymbol{x})$ that is defined by its self-similarity. The kernel can be decomposed into two components: one that describes decay of weight versus distance and one that describes the proportion of correlation weight in every direction. The latter portion is called the mixing measure, which *Benson et al.* [2006] applied to the function $\hat{\varphi}(\boldsymbol{k})$, the convolution kernel in Fourier space at any wave vector $\boldsymbol{k}$. It is unclear exactly how this angular dependence in Fourier space corresponds to the true angular dependence in real space. In this paper, we apply the mixing measure directly to the function $\varphi(\boldsymbol{x})$, the convolution kernel in real space. In this way the effect on the directionality in K-structure is clear. Additionally, *Benson et al.* [2006] presented the results of solute transport through single realizations of operator-scaling random fields, in order to compare directly between realizations with slightly different structure. However, their results cannot be translated to the statistical behavior of the ensemble mean transport. Ensemble results are presented for all examples in this paper, making all results more robust and directly comparable to analytic theories developed using the ergodic hypothesis. We also investigate deviations of individual realizations from the ensemble.

The fields used in this study have two advantages over classical, isotropic fBm fields: 1) the operator-scaling fields are described by matrix scaling values which allow different scaling (or different Hurst coefficients) in different directions; and, 2) the mixing measure $M(\theta)$ accommodates any discretization on the radius of isotropy, allowing completely user-defined directionality in K-structure. The fast Fourier transform (FFT) method is used, allowing rapid generation of large fBm fields.

3. Mathematical Background

Here we give a brief overview of the generation and correlation structure of operator-scaling random fields. *Biermé et al.* [2007] give a more rigorous derivation of the mathematical properties of multidimensional fractional Brownian motion (fBm) $B_H(x)$. In order to describe the properties of an fBm, we must first define the properties of the related fractional Gaussian noise (fGn) $G(x,h) = B_H(x+h) - B_H(x)$. In one dimension (1-$d$), an fGn is statistically invariant under self-affine transformations: the random variables $G(x, rh)$ and $r^H G(x,h)$ have the same Gaussian distribution [*Molz et al.*, 1997]. The scalar H is the celebrated Hurst scaling coefficient. The fGn is also statistically homogeneous: $G(x,h)$ has the same distribution as $G(x+r,h)$ for any separation r.

A finite approximation of the continuous d-dimensional isotropic fBm can be created by multiplying the Fourier filter with the scaling properties $\hat{\varphi}(c\boldsymbol{k}) = c^{-A}\hat{\varphi}(\boldsymbol{k})$ against a Gaussian white noise in the spectral representation, where $\boldsymbol{k}$ is a wave vector. This relationship is satisfied by a simple power law: $\hat{\varphi}(\boldsymbol{k}) = |\boldsymbol{k}|^{-A}$. Multiplying by this filter in Fourier space defines the operation of fractional-order integration. In this isotropically scaling case in d-dimensions, the order of integration, A, is related to the Hurst coefficient, by $A = H + d/2$, with $0 < H < 1$ [*Benson et al.*, 2006]. A random field that has different scaling rates in different directions can be generated by using a matrix-valued rescaling of space: $\hat{\varphi}(c^{\boldsymbol{Q}}\boldsymbol{k}) = c^{-A}\hat{\varphi}(\boldsymbol{k})$. The matrix $\boldsymbol{Q}$ defines the deviation from the isotropic case in which $\boldsymbol{Q} = \boldsymbol{I}$, the $d \times d$ identity matrix [*Benson et al.*, 2006]. The matrix power $c^{\boldsymbol{Q}}$ is defined by a Taylor series $[c^{\boldsymbol{Q}} = \exp(\boldsymbol{Q}\ln c) = \boldsymbol{I} + \boldsymbol{Q}\ln c + \frac{(\boldsymbol{Q}\ln c)^2}{2!} + \frac{(\boldsymbol{Q}\ln c)^3}{3!} + ...]$. The scaling relation for the convolution kernel in Fourier space is given in *Benson et al.* [2006]: $\hat{\varphi}(c^{\boldsymbol{Q}}\boldsymbol{k}) = c^{-A}\hat{\varphi}(\boldsymbol{k})$. We can use the Fourier inversion formula $\varphi(\boldsymbol{x}) = \frac{1}{2\pi}\int e^{i\boldsymbol{k}\cdot\boldsymbol{x}}\hat{\varphi}(\boldsymbol{k})d\boldsymbol{k}$ to find the scaling relation in real space. We assume here that $\boldsymbol{Q}$ is a diagonal matrix (implying orthogonal eigenvectors):

$$\begin{aligned}\varphi(c^{\boldsymbol{Q}}\boldsymbol{x}) &= \frac{1}{2\pi}\int e^{i\boldsymbol{k}\cdot(c^{\boldsymbol{Q}}\boldsymbol{x})}\hat{\varphi}(\boldsymbol{k})d\boldsymbol{k} \\ &= \frac{1}{2\pi}\int e^{ic^{\boldsymbol{Q}}\boldsymbol{k}\cdot\boldsymbol{x}}\hat{\varphi}(\boldsymbol{k})d\boldsymbol{k}.\end{aligned}$$

Make the substitution $c^{\boldsymbol{Q}}\boldsymbol{k} = \boldsymbol{z}$, therefore $\boldsymbol{k} = [c^{\boldsymbol{Q}}]^{-1}\boldsymbol{z} = c^{-\boldsymbol{Q}}\boldsymbol{z}$ and $d\boldsymbol{k} = |c^{-\boldsymbol{Q}}|d\boldsymbol{z}$.

$$\begin{aligned}\varphi(c^{\boldsymbol{Q}}\boldsymbol{x}) &= \frac{1}{2\pi}\int e^{i\boldsymbol{z}\cdot\boldsymbol{x}}\hat{\varphi}(c^{-\boldsymbol{Q}}\boldsymbol{z})|c^{-\boldsymbol{Q}}|d\boldsymbol{z} \\ &= \frac{1}{2\pi}\int e^{i\boldsymbol{z}\cdot\boldsymbol{x}}c^{A}\hat{\varphi}(\boldsymbol{z})|c^{-\boldsymbol{Q}}|d\boldsymbol{z} \\ &= c^{A}|c^{-\boldsymbol{Q}}|\varphi(\boldsymbol{x}).\end{aligned}$$

Recognizing that $A = H + \frac{d}{2}$ and $|c^{-\boldsymbol{Q}}| = c^{\mathrm{tr}(-\boldsymbol{Q})}$ we arrive at the scaling relation for the convolution kernel in real space: $\varphi(c^{\boldsymbol{Q}}\boldsymbol{x}) = c^{H+d/2+\mathrm{tr}(-\boldsymbol{Q})}\varphi(\boldsymbol{x})$ where tr() is the trace of the matrix, or sum of the eigenvalues. In this setting, we assume $\mathrm{tr}(\boldsymbol{Q}) = d$, so the scaling relationship simplifies to

$$\varphi(c^{\boldsymbol{Q}}\boldsymbol{x}) = c^{H-d/2}\varphi(\boldsymbol{x}). \tag{1}$$

Any function satisfying the scaling relationship in (1) can be used to create an operator-scaling fBm (osfBm) $B_\varphi(\boldsymbol{x})$ by convolving (in a discrete Fourier transform sense) the kernel with uncorrelated Gaussian noise: $B_\varphi(\boldsymbol{x}) = B(\boldsymbol{x}) \star \varphi(\boldsymbol{x})$. The convolution product will have the self-affine distributional property:

$$B_\varphi(c^{\boldsymbol{Q}}\boldsymbol{x}) = c^{H}B_\varphi(\boldsymbol{x}) \tag{2}$$

This equation specifies that the osfBm resembles itself (statistically) after a rescaling in which space is stretched more in one direction than another. For simplicity, in this paper we present operator-scaling fields with orthogonal eigenvectors (diagonal matrix $\boldsymbol{Q}$), although this is not a requirement. We break the scaling function into the power-law versus "distance" component and the radial "weights" that define the strength of statistical dependence in any direction. For example, a simple 2-D convolution kernel that satisfies this is:

$$\varphi(\boldsymbol{x}) = M(\theta)[c_1|x_1|^{2/q_1} + c_2|x_2|^{2/q_2}]^{(H-1)/2} \tag{3}$$

where q_1 and q_2 are the diagonal components of $\boldsymbol{Q}$ ($q_1 + q_2 = d = 2$). Constants $c_1 = [R]^{-2/q_1}$ and $c_2 = [R]^{-2/q_2}$ are defined in terms of R, the "radius of isotropy". These constants allow for the possibility that different units may be used to measure the fields, such that the radius of isotropy R can have any value and any length units. $M(\theta)$ is an arbitrary measure of the directional weight, which is user-defined on the radius of isotropy corresponding to $|\boldsymbol{x}| = R$.

When creating the kernel, the directional weights $M(\theta)$ must be stretched anisotropically according to the matrix

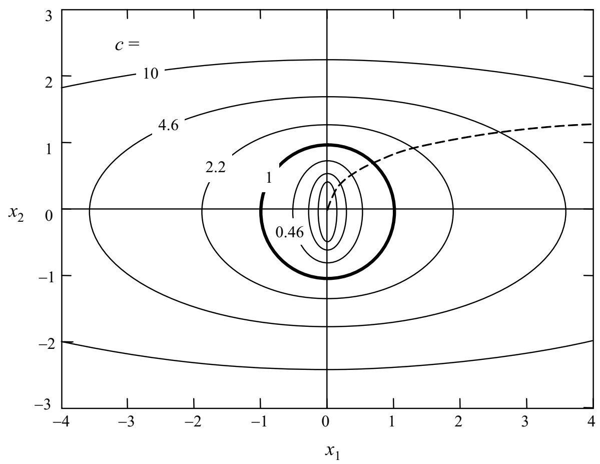

$$Q = \begin{bmatrix} 0.6 & 0 \\ 0 & 1.4 \end{bmatrix} \qquad c^Q = \begin{bmatrix} c^{0.6} & 0 \\ 0 & c^{1.4} \end{bmatrix}$$

Figure 1. Matrix stretching (and contraction) of the curve defined by the "radius of isotropy" (or "curve of isotropy"), $R = 1$ (from *Benson et al.*, [2006]). The dashed line shows the mapping of the point $M(\theta = \pi/4)$ by the matrix rescaling of space $c^{\boldsymbol{Q}}\boldsymbol{x}$. Points on this dashed line follow $(x_1, x_2) = c^{\boldsymbol{Q}}(\frac{1}{\sqrt{2}}, \frac{1}{\sqrt{2}})$ for all $c \geq 0$.

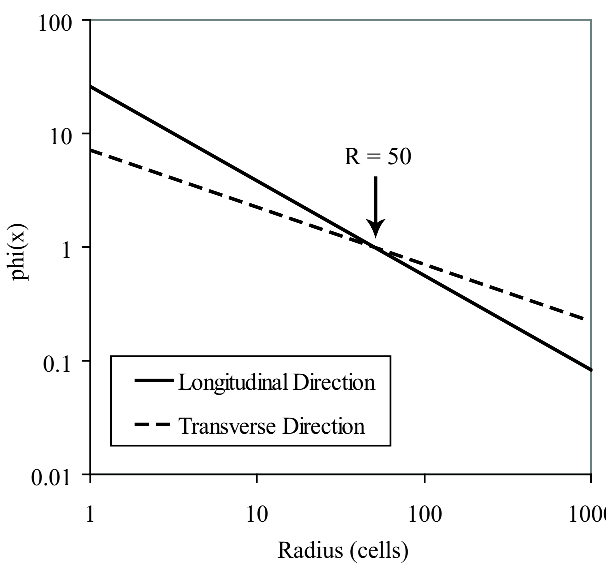

Figure 2. One-dimensional transects of $\varphi(\boldsymbol{x})$ ($H_{longitudinal} = 0.5$, $H_{transverse} = 0.3$, isotropic mixing measure). Intersection of the one-dimensional osfBm transects defines the radius of isotropy $R = 50$. Such a method could be used to determine the radius of isotropy from the correlation function of a well defined data set.

$\boldsymbol{Q}$. Figure 1 demonstrates how the geometry of the convolution kernel is induced by the scaling matrix $\boldsymbol{Q}$ according to the relationship:

$$(x_1, x_2) = c^{\boldsymbol{Q}}(y_1, y_2) \tag{4}$$

for all $c \geq 0$ and $\sqrt{y_1^2 + y_2^2} = R$ (radius of isotropy). This relation allows the tracing of angular sections of the curve of isotropy that define the mixing measure into a "stretched" space defined by the operator-scaling relationship. In other words, for the operator-scaling relationship (2) to be fulfilled, the weight function is stretched more in one direction than another. Therefore, the function $M(\theta)$ specifies weights (a discrete or continuous measure) along the curve of isotropy $|\boldsymbol{x}| = R$. These weights are then transferred along curves such as the dashed line in Figure 1. It is a simple matter to separately calculate the value of the power law portion (in (3)) at every point $\boldsymbol{x}$ and multiply the two functions. In this example, the x_1 direction is stretched outside of the radius of isotropy and compressed inside. Just the opposite is true for the x_2 direction. This implies that the chosen radius of isotropy is very important to both measurement and simulation of osfBm fields. This issue does not arise in the isotropic case with a uniform rescaling of

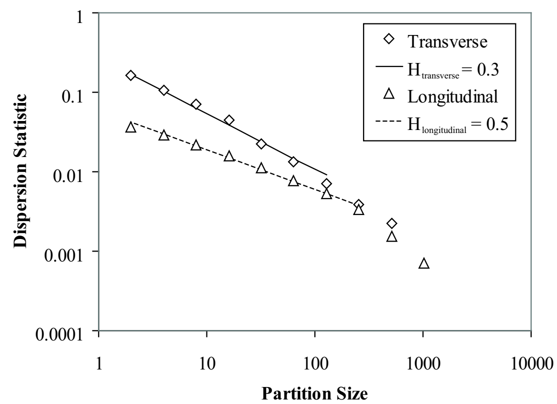

Figure 3. Ensemble dispersional analysis of a $ln(K)$ field in the longitudinal and transverse directions, 1024×512 respectively. The fields were created with the braided measure, $H_{longitudinal} = 0.5$, $H_{transverse} = 0.3$, and radius of isotropy $R = 1000$ (explained in section 4.3). Both directions follow the expected slope of $H - 1$ in log-log space for small partitions.

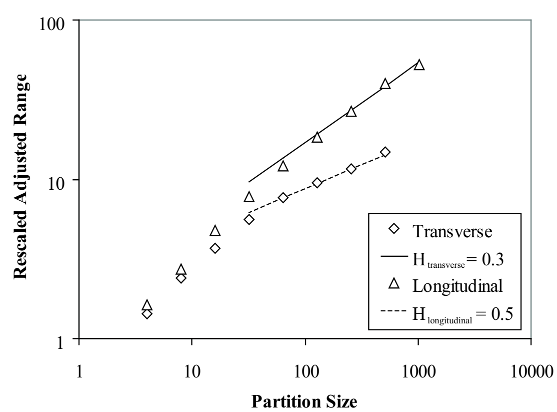

Figure 4. Ensemble rescaled range (R/S) analysis of a $ln(K)$ field in the longitudinal and transverse directions, 1024×512 respectively. The fields were created with the braided measure, $H_{longitudinal} = 0.5$, $H_{transverse} = 0.3$, and radius of isotropy $R = 1000$ (explained in section 4.3). Both directions follow the expected slope of H in log-log space for large partitions.

space. We note that the completely general $M(\theta)$ is a novel anisotropic spatial weighting even in the isotropically scaling case. We investigate the effect of changing the radius of isotropy R below.

3.1. Fast Fourier Transform Convolution

Numerical evaluation of a convolution integral in multiple dimensions is, in general, very computationally intensive. For this reason, we make use of the theorem:

$$\mathcal{F}^{-1}[\mathcal{F}(\varphi(\boldsymbol{x}))\mathcal{F}(B(\boldsymbol{x}))] = \varphi(\boldsymbol{x}) \star B(\boldsymbol{x}) \qquad (5)$$

Here we define the kernel $\varphi(\boldsymbol{x})$ and a d-dimensional sequence of uncorrelated Gaussian random variables $B(\boldsymbol{x})$, and Fourier transform $\mathcal{F}$, and inverse transform $\mathcal{F}^{-1}$. The Fast Fourier Transform (FFT) algorithm is used to efficiently calculate the Fourier transforms. The FFT method has commonly been used for artificial generation of fBm [e.g. *Hassan et al.*, 1997; *Benson et al.*, 2006]; however, some researchers have suggested problems with this method of generation for fBm. *Bruining et al.* [1997] found that the Fourier transform method for generating fBm failed to produce the correct statistical properties. *Bruining et al.* observed that fBm generated by the FFT method did not produce the expected standard deviation of the means for various partitions. This could be a result of the small size (64×64) of the fields investigated. It has been noted (e.g., *Caccia et al.* [1997]) that longer series $(N \geq 1024)$ are necessary for accurate estimation of the Hurst coefficient.

To verify the correct fractal behavior of the operator-scaling random fields created by the FFT method, we sampled the fields along the orthogonal eigenvectors. If $B_\varphi(\boldsymbol{x})$ is an osfBm then it must obey the scaling relation in (2) for all $c > 0$. If $\boldsymbol{u}$ is an eigenvector of $\boldsymbol{Q}$ with eigenvalue q_i then $c^{\boldsymbol{Q}}\boldsymbol{u} = c^{q_1}\boldsymbol{u}$, and substituting this into (2), we have $B_\varphi(c^{q_1}\boldsymbol{u}) = c^H B_\varphi(\boldsymbol{u})$, and after a substitution $r = c^{q_1}$:

$$B_\varphi(r\boldsymbol{u}) = r^{H/q_1} B_\varphi(\boldsymbol{u}) \qquad (6)$$

Therefore, in the direction of an eigenvector with eigenvalue q_i (and only in this direction), a one-dimensional transect of an osfBm is a self-similar fBm with scaling coefficient H/q_i. We assume that the sum of the positive eigenvalues of $\boldsymbol{Q}$ equals the Euclidean number of dimensions.

We use dispersional analysis and rescaled range analysis applied to 1-d transects of data taken in the directions of the eigenvectors to estimate the Hurst coefficient(s). The fields must be sampled along the eigenvectors, or traditional methods of H estimation are not valid. *Caccia et al.* [1997] found dispersional analysis to be an accurate measure of the scaling behavior of fGn for smaller partition sizes (the largest partition sizes typically fall off from the linear behavior in log-log space). Dispersional analysis uses the standard deviation of the means for different partition sizes to quantify the scaling behavior of an fGn. Dispersional analysis of the increments of the one-dimensional transects was used to ensure the correct scaling properties of typical osfBm at the smaller partition sizes (Figure 3). The slope of the dispersion statistic versus the partition size in a log-log plot is $H - 1$ [*Caccia et al.*, 1997].

As with dispersional analysis, rescaled range analysis involves calculating a local statistic for each partition size. The rescaled range (R/S) statistic is the range of the values in the partition divided by the standard deviation of the values in the partition. *Mandelbrot* [1969b] found rescaled range analysis to be a robust measure of long-run statistical dependence. R/S analysis serves as a compliment to dispersional analysis, since it is most reliable for larger partition sizes [*Caccia et al.*, 1997]. In log-log space, the slope of the rescaled range statistic versus partition size should equal the Hurst coefficient along each eigenvector (Figure 4).

For all ensemble simulations presented, 100 realizations were generated, each with a different "random" input Gaussian noise. The 2-D input noise and the convolution kernel were 2048×1024 arrays. The noise and the kernel were both transformed via FFT, multiplied together, then inverse transformed to create the convolution as described in the previous section. The middle 1/4 of each field was subsampled for transport simulation (in order to minimize periodic effects from the FFT) leaving a field with dimensions 1024 by 512 cells. It is typical to subsample the fields when synthetically generating an fBm. *Lu et al.* [2003] also found it necessary to subsample fields created by the successive random additions (SRA) method due to irregularities near the boundaries of the domain.

4. Transport Simulation Results

MODFLOW was used to solve for the velocity field assuming an average hydraulic gradient across the fields of 0.01, with no-flow boundaries at the top and bottom of the field. Using *LaBolle et al.'s* [1996] particle tracking code, 100,000 particles were released in each field, spaced evenly between points 128 and 384 along the high head side of the fields to avoid lateral boundary effects on transport (giving a total of 10,000,000 particles for each ensemble of 100 realizations). The local dispersion and diffusion were set to zero to most closely match the analytical assumptions of *Di Federico and Neuman* [1998b]: *Benson et al.* [2006] found that small local dispersivities did not appreciably change the growth rates of single plumes; however, *Hassan et al.* [1997] found that fairly large local dispersivity noticeably changed the plume shapes. *Kapoor and Gelhar* [1994b] showed that although local dispersion is important to the destruction of the spatial variance of concentration in heterogeneous aquifers, local dispersion does not appreciably affect the longitudinal spatial second moment or the macrodispersivity. For this study, we modeled purely advective transport as we were most interested in testing analytic predictions of longitudinal macrodispersivity in fractal fields. The effect of local dispersion on individual and ensemble plumes is part of an ongoing study.

We monitored the plume evolution at logarithmic time steps to observe growth across many scales, as well as the earliest and latest breakthrough. Particle breakthrough rates were recorded, as well as longitudinal concentration profiles, computed by summing the particles in each transverse row of cells at each time step. Additionally, the first and second longitudinal moments of the plumes were recorded and used to calculate apparent dispersivity (α_L) of the ensemble plumes, calculated using the formula $2\alpha_L = d(VAR(X))/d\bar{X}$, where X are the particle positions, and $VAR(X)$ is the variance of the particle positions in the longitudinal direction, calculated at each time step by the particle tracking code. First differences of $VAR(X)$ were used to approximate the derivative. Transverse dispersion was not addressed as the main goal of this paper is a comparison with analytic predictions of longitudinal dispersivity in fractal fields.

4.1. Transport in Isotropic fBm Fields

Beginning with a simple case, we explored the effects of the Hurst coefficient on transport in purely isotropic fBm fields (uniform mixing measure $M(\theta) = \frac{1}{2\pi}$ with $\boldsymbol{Q} = \boldsymbol{I}$, the identity matrix). The K fields were adjusted to be lognormally distributed with mean and standard deviations $\mu_{\ln(K)} = 0$ and $\sigma_{\ln(K)} = 1.5$. For small mean travel distances, the observed ensemble average dispersivity (relative or effective dispersivity) follows ballistic growth: a superposition of advective transport in a stratified conductivity field, characterized by a linear growth of apparent dispersivity with mean travel distance (Figure 5). In each case, ($H = 0.2, 0.5$, and 0.8), the dispersivity drops to sublinear (but still super-Fickian) growth at larger mean travel distances. Counter-intuitively, the $\ln(K)$ field with the least persistence ($H = 0.2$) engendered greater spreading rates at the earliest time. We attribute this result to the greater small-scale heterogeneities at lower H (due to less correlation). The initial width of the plume samples more heterogeneity for smaller H due to less correlation in the K field, which results in more dispersion at early times. At larger mean travel distances, the growth of effective dispersivity versus mean distance also follows a power law, with a lower exponent for a lower value of H. It is logical that lower H should lead to less dispersivity at large travel distances, due to less correlation and less large-scale heterogeneities. At long travel distances our results agree qualitatively with *Kemblowski and Wen's* [1993] and *Zhan and Wheatcraft's* [1996] calculations for fractal stratified aquifers that dispersion should decrease for smaller Hurst coefficients. These papers predicted roughly linear growth of dispersivity versus mean travel distance, which falls off from linear growth and approaches a constant (Fickian) value as the travel distance approaches the maximum length scale (L_{max}). Our plume mean distances do not approach the largest wavelength, which is larger than the domain size. However, for a lower Hurst coefficient, their analyses predict an earlier transition to sub-linear growth, which we also observe.

Neuman [1995], *Rajaram and Gelhar* [1995], and *Di Federico and Neuman* [1998b] predict the spreading of plumes in isotropic fractal K-fields similar to those in our experiments. Their predictions are based only on the Hurst coefficient in the longitudinal direction. *Di Federico and Neuman* [1998b] predict that a plume traveling in a fractal field with no fractal cutoff will exhibit permanently pre-asymptotic growth, with a longitudinal macrodispersivity (α_L) that evolves according to $\alpha_L \propto \bar{X}^{1+2H}$ for mean travel distance $\bar{X}$ and longitudinal Hurst coefficient H. *Rajaram and Gelhar* [1995] predict that plume growth in an fBm K-field will exhibit a macrodispersivity according to $\alpha_L \propto \bar{X}^H$ from a two-particle, relative dispersion approach. *Di Federico and Neuman* predict that if the plume growth exceeds the fractal cutoff (the plume is no longer continually sampling larger scales of heterogeneity) then there will be a transition to a Fickian growth rate ($\alpha_L = const.$). Mercado [1967] describes a perfectly stratified model with no mixing between layers. This ballistic motion will exhibit linear growth of apparent macrodispersivity verses travel distance ($\alpha_L \propto \bar{X}$).

Our results for isotropic fBm fields show a much weaker dependence on H than the predictions for growth of macrodispersivity (α_L) by *Rajaram and Gelhar* [1995], who predicted a growth of macrodispersivity following the relation $\alpha_L \propto \bar{X}^H$. None of the plumes approach *Di Federico and Neuman's* [1998b] prediction of super-linear and permanent pre-asymptotic growth, $\alpha_L \propto \bar{X}^{1+2H}$. The observed ensemble average plume growth agrees qualitatively with the predictions by *Rajaram and Gelhar* [1995] that anomalous dispersion is limited to linear or sublinear growth of dispersivity.

In addition to longitudinal plume dispersion, we also investigated the longitudinal dispersivity of plume centroids (Figure 5). The dispersivity of plume centroids grows linearly in fBm fields. For larger Hurst coefficients, the dispersivity grows at a faster (but still linear) rate. We can therefore infer that there is more uncertainty in plume location in fractal fields with higher Hurst coefficients. For higher values of the Hurst coefficient a larger portion of the total ensemble dispersivity is a result of the dispersivity of the plume centroids, indicating more realization-to-realization variability. Lower values of the Hurst coefficient describe fields with more small scale heterogeneity and less realization-to-realization variability. As a result, more of the ensemble dispersivity is a result of the spreading of individual plumes for lower Hurst coefficients. The dispersivity of the ensemble plume is equal to the sum of the effective dispersivity and the dispersivity of the plume centroids. The behavior of the ensemble plume dispersivity was found to be very similar to that of the effective dispersivity (ensemble average dispersivity) as the dispersivity of the plume centroids is much smaller than the effective dispersivity.

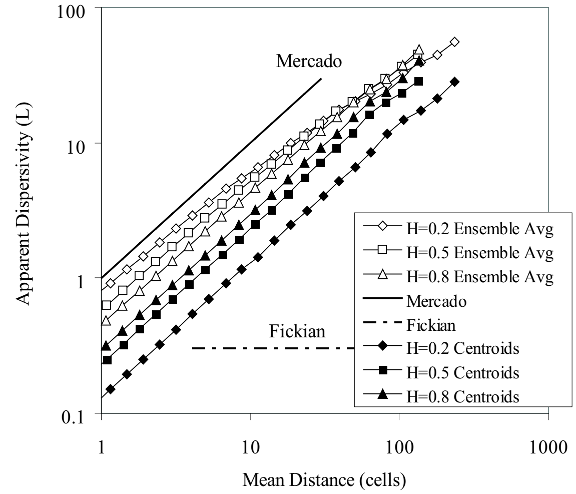

Figure 5. Apparent dispersivity versus mean travel distance for several values of the Hurst coefficient in the purely isotropic case (constant mixing measure with no matrix rescaling). Results are plotted for both the ensemble average plume dispersivity (effective dispersivity) and the dispersivity of the plume centroids.

4.2. Effects of the Mixing Measure

The mixing measure specifies the strength of correlation in any direction. In essence this amounts to a prefactor on the power law correlation in any direction. Most previous research (numerical and analytical) has focused on the effect of the scaling exponent on growth rate. To explore the effects of different mixing measures, or weight functions $M(\theta)$, ensemble simulations were run with 2-D random osfBm fields. Typical values of the Hurst coefficients were used: 0.5 in the horizontal (direction of transport) and 0.3 in the vertical or transverse direction. Although there is a great deal

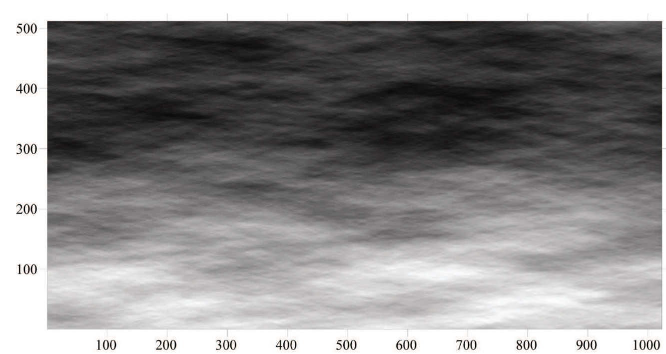

Figure 6. One realization of an osfBm with $H_{longitudinal} = 0.7$, $H_{transverse} = 0.9$, elliptical mixing measure, $R = 50$

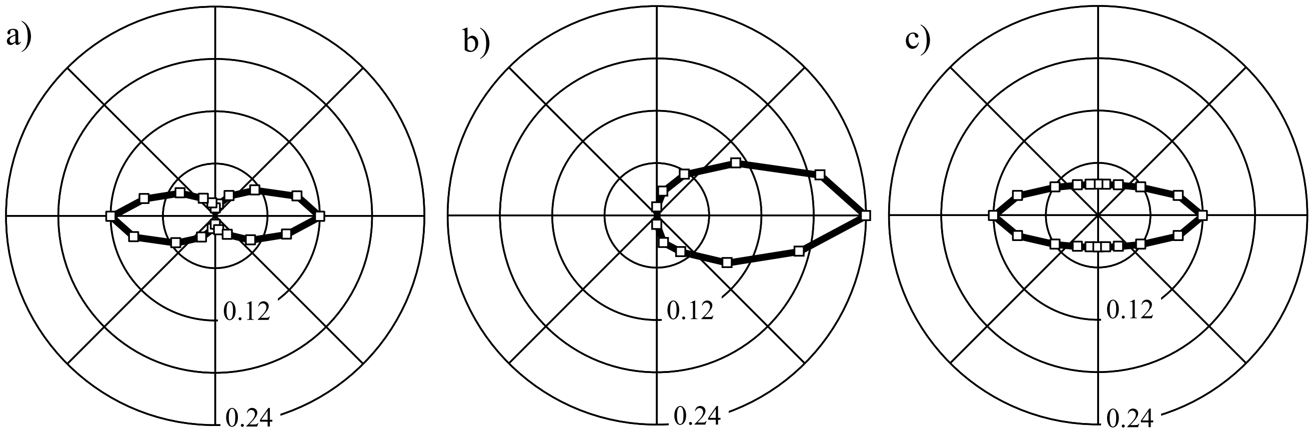

Figure 7. Anisotropic mixing measures presented by *Benson et al.* [2006]: a) "braided stream" b) "downstream" c) "elliptical". $M(\theta)$ is discretized into 20 sections on the radius of isotropy.

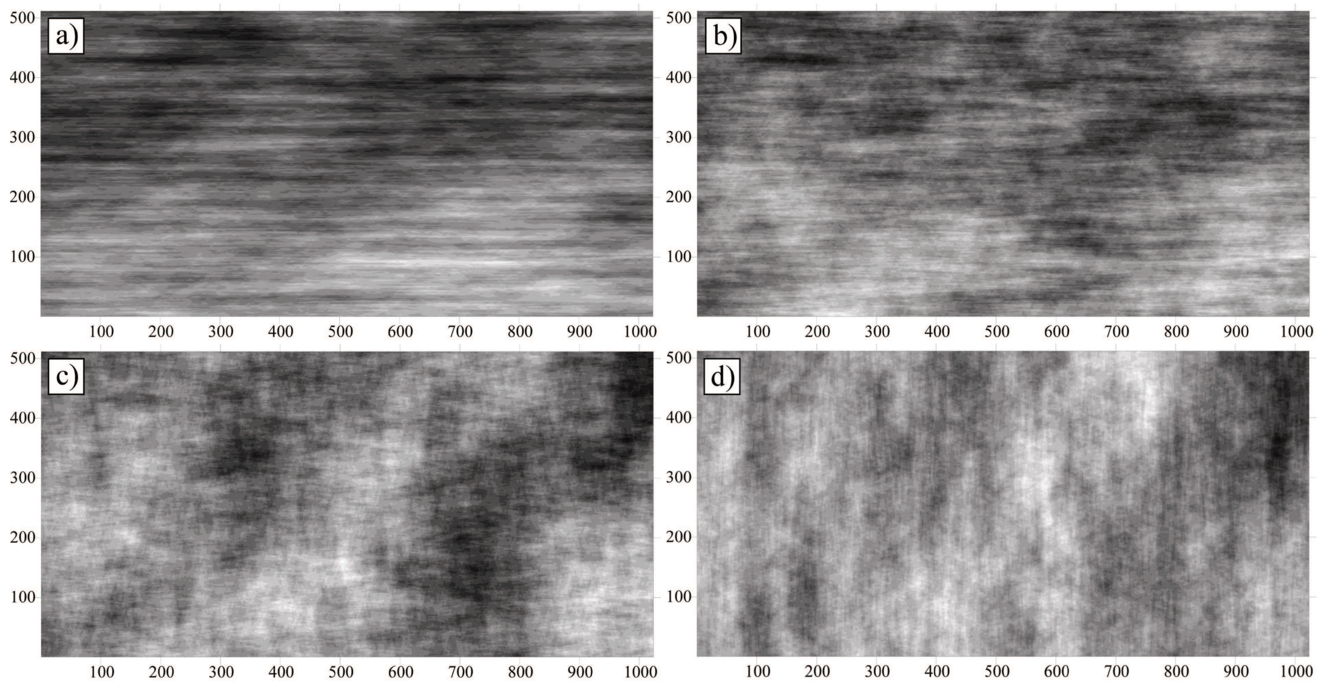

Figure 8. Log(K) fields with identical scaling behavior ($H_{longitudinal} = 0.5$, $H_{transverse} = 0.3$, elliptical mixing measure) but varying radius of isotropy (R). a) $R = 1000$, b) $R = 100$, c) $R = 10$, d) $R = 1$

of variability in measured values of H from boreholes and other methods (see *Benson et al.* [2006] for a review of many of the site investigations) these values for the horizontal and vertical Hurst coefficients appear to be reasonable, middle-of-the-road values. The K fields were adjusted to be lognormally distributed with mean and standard deviations $\mu_{ln(K)} = 0$ and $\sigma_{ln(K)} = 1.5$. Ensemble results for the "braided stream", "downstream", "elliptical", (see Figure 7) and uniform measure ($M(\theta) = 1/2\pi$) (all from *Benson et al.* [2006]) were compared. The "braided stream" measure was constructed from a histogram of stream channel directions. The "downstream" measure is only the downstream components of the braided stream measure. The "elliptical" measure is a classical elliptical set of weights with the major axis aligned with the direction of transport.

The effects of these mixing measures on the breakthrough and dispersion are fairly predictable, and are not shown in any plots. The braided and downstream measures create K-fields with continuity that resembles the braided stream which is the origin for the measure. The elliptical measure produces a somewhat smoother continuity in the hydraulic conductivity field (Figure 6). The uniform measure is the only one that produces a significantly different K-field, due to the much greater weight in the transverse direction. In general, more weight in the longitudinal direction creates more continuity in the structure of the K-field, leading to earlier breakthrough, and increased dispersivity vs. mean travel distance. The effects of the mixing measure were observed to be small in comparison to the effects of the orthogonal Hurst coefficients, and the chosen radius of isotropy, discussed immediately.

4.3. Effects of Radius of Isotropy

In the case of anisotropic matrix rescaling (osfBm), the chosen radius of isotropy (R) is extremely important. The weighting function is rescaled according to Figure 1. As a result, for the same $H_{longitudinal}$ and $H_{transverse}$ we may observe very different correlation structures depending on whether we are inside or outside of the radius of isotropy (Figure 8).

In studies that investigate the anisotropic scaling of the properties of sedimentary rocks [e.g. *Hewett*, 1986; *Castle et al.*, 2004; *Liu and Molz*, 1997a; *Molz and Boman*, 1993, 1995; *Tennekoon et al.*, 2003] the typical assumption has been that determining the scaling behavior, or Hurst coefficients, in orthogonal directions (assumed to be the eigenvectors of H) is sufficient to describe the structure of the aquifer. However, fields with the same orthogonal Hurst coefficients may describe extremely different correlation structures at scales smaller or larger than the radius of isotropy (Figure 8). These unique correlation structures also significantly affect plume growth (Figures 9 and 10). Visual inspection of the osfBm fields (Fig. 8) demonstrates that many of the possible osfBm fields do not resemble typical aquifer hydraulic conductivity. However, some appear to represent many of the features of say, braided stream systems, with narrow windows of directional continuity, bifurcating high-K zones, and long-range continuity of both high- and low-K units (Figure 6).

Methods for determining the radius of isotropy from real data may be developed. In Figure 2 we see one-dimensional transects of $\varphi(\boldsymbol{x})$, which can be directly calculated from the auto-correlation function [*Molz et al.*, 1997] which can be estimated for a real data set. With a uniform mixing measure, we observe the radius of isotropy, $R = 50$, at the intersection of the two transects (Figure 2). A non-uniform mixing measure could complicate such observations. Future research could develop more advanced methods for experimental determination of the radius of isotropy in osfBm fields.

The effective longitudinal dispersivity appears to be limited to linear or sublinear growth with respect to mean travel distance for all osfBm fields (Fig. 9). The magnitudes of α_L at any mean travel distance range over nearly an order-of-magnitude, but none exceed linear growth. For most of the simulations, we do not plot values of α_L beyond a mean travel distance of approximately 100 cells. The plots are cut off as soon as the first leading particles reach the domain boundary at $x_1 = 1024$, since the plume variance can no longer be accurately calculated. In the ensemble case, the leading particles may have traveled as much as an order-of-magnitude farther than the plume centroid. Even though the $\sigma_{ln(K)}$ was fairly small at 1.5, the ensemble plumes are highly non-Gaussian (Figure 11) and cannot be modeled by a classical, local, second-order, advection-dispersion equation.

Similar to the case of classical isotropic fBm fields, the plume centroid dispersivity was found to be limited to linear growth with mean centroid displacement. The slope of the linear growth is dependent on the correlation structure and therefore depends on the orthogonal Hurst coefficients as well as the unit circle radius.

Benson et al. [2006] made observations concerning the effects of the transverse Hurst coefficient on plume growth. The authors found that higher transverse Hurst coefficients created more continuity in the K fields, which led to faster

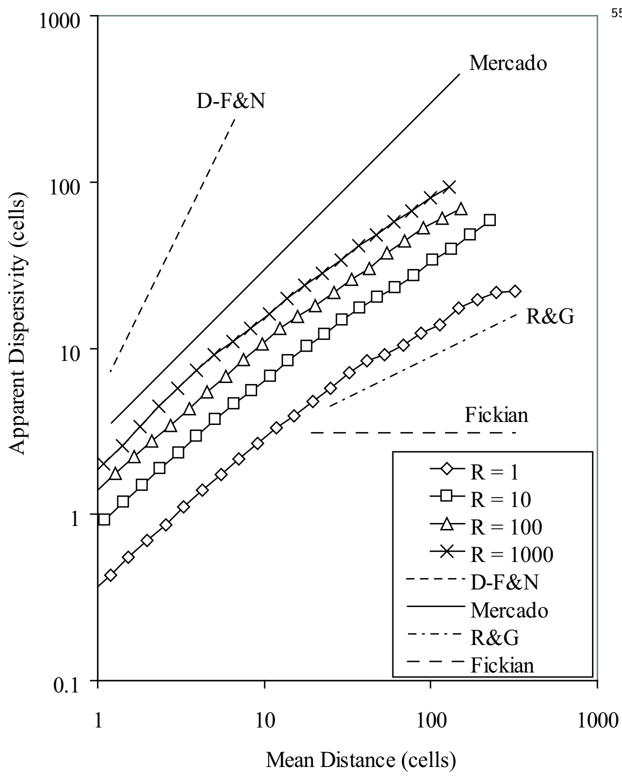

Figure 9. Effective dispersivity versus mean travel distance for ensemble plumes in Log(K) fields with identical scaling behavior ($H_{longitudinal} = 0.5$, $H_{transverse} = 0.3$, elliptical mixing measure) but varying radius of isotropy (R). The analytic growth rates predicted by *Di Federico and Neuman* (D-F&N) [1998b], *Mercado* [1967], and *Rajaram and Gelhar* (R&G) [1995] are also plotted.

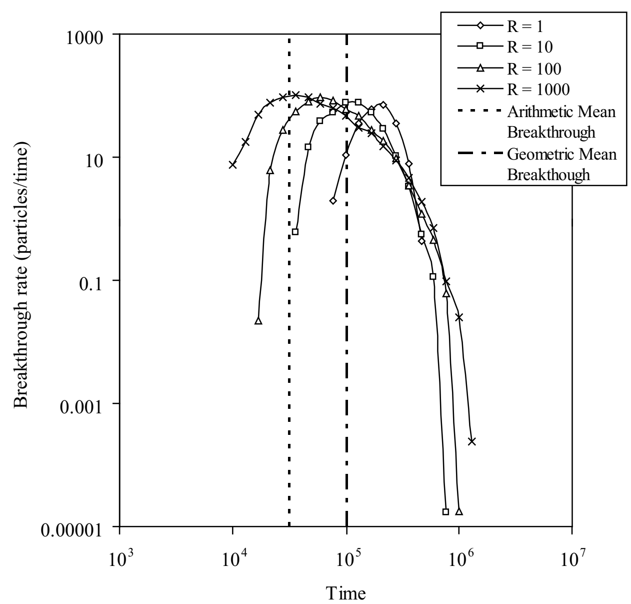

Figure 10. Normalized breakthrough curves for ensemble plumes in ln(K) fields with identical scaling behavior ($H_{longitudinal} = 0.5$, $H_{transverse} = 0.3$, elliptical mixing measure) but varying radius of isotropy (R). The arithmetic mean and geometric mean breakthrough times are also plotted. The arithmetic mean hydraulic conductivity is simply the average of all the K values in the field. The geometric mean is the *nth* root of n numbers—the geometric mean K is smaller than the arithmetic mean K, which leads to a later geometric mean breakthrough.

plume growth. The added complication of the effects of the radius of isotropy make such a general observation impossible. Nonetheless, we do observe that 1) both the transverse and longitudinal Hurst coefficients as well as the radius of isotropy are important to transport, and 2) all ensemble transport in 2-d osfBm fields is limited to sub-Mercado growth rates.

5. Comparison with Analytic Predictions

None of the plumes (in either the classical isotropic case or the anisotropic operator-scaling case) demonstrate asymptotic or Fickian-type growth (Figures 5 and 9), a result that agrees with the analytic theories, as the plume size never exceeds the scale of the largest heterogeneities present. All of the ensemble results exhibit primarily Mercado-type plume growth. None of the results follow *Di Federico and Neuman's* permanently pre-asymptotic growth. Simulations were conducted with various longitudinal and transverse Hurst coefficients (results are not shown for brevity). These ensemble results also demonstrated primarily Mercado-type plume growth. In all of the experiments conducted, the ensemble average plume growth through the osfBm $\log(K)$ fields does not exceed Mercado's stratified result. This includes cases in which $\sigma_{ln(K)}$ is reduced to 0.01 to better coincide with small perturbation requirements of the analytic theories. In addition to the ensemble results, an examination of the growth rates of individual realizations gave very similar results (Figure 12). None of the individual plumes sustain super-Mercado growth, and none of the plumes converge to a Fickian regime.

Berkowitz et al. [2006] briefly discuss analytic results for transport in fields with large correlation lengths, including the "racetrack" model (a perfectly stratified aquifer). Although these fields demonstrate super-Fickian plume growth, *Berkowitz et al.* [2006] point out that it cannot be considered anomalous transport as it is merely a superposition of normal transport in each layer. In the case of purely advective transport in a stratified aquifer, dispersivity should grow with $\bar{X}$, similar to our results. *Matheron and de Marsily* [1980] found that dispersivity grows with $t^{1/2}$ in the presence of diffusion between layers. Since the long-range continuity inherent in our osfBm fields clearly engenders very stratified flow, we might expect *Matheron and de Marsily's* result if local diffusion or dispersion is included in our simulations; however, this has not yet been investigated.

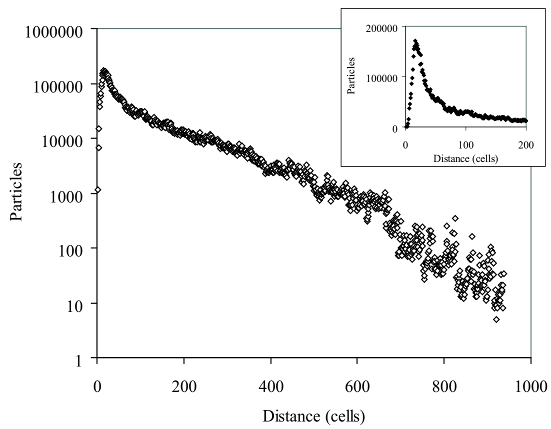

Figure 11. Semi-log plot of ensemble longitudinal plume profile (insert: plume profile in real space). We see a plume shape has a very fast leading edge that is highly non-Gaussian for this case with $H_{longitudinal} = 0.7$, $H_{transverse} = 0.9$, elliptical measure, $R = 50$ (same as Figure 6). The K-fields were constructed with $\mu_{ln(K)} = 0$ and $\sigma_{ln(K)} = 1.5$. The leading edge of the ensemble plume decays slower than the Gaussian at approximately an exponential rate.

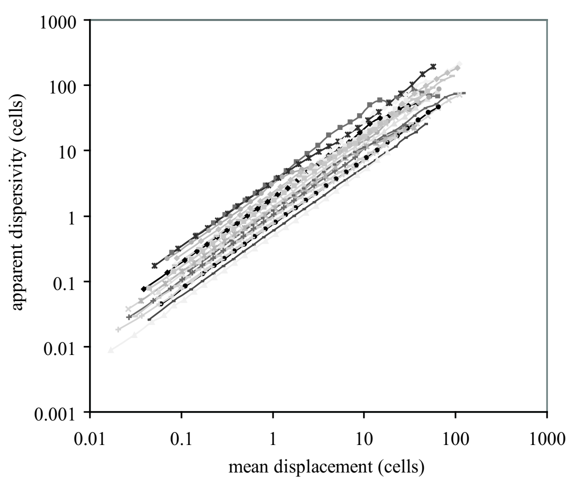

Figure 12. Apparent dispersivity for 20 individual plume realizations. No individual plumes exhibit sustained super-Mercado growth rates.

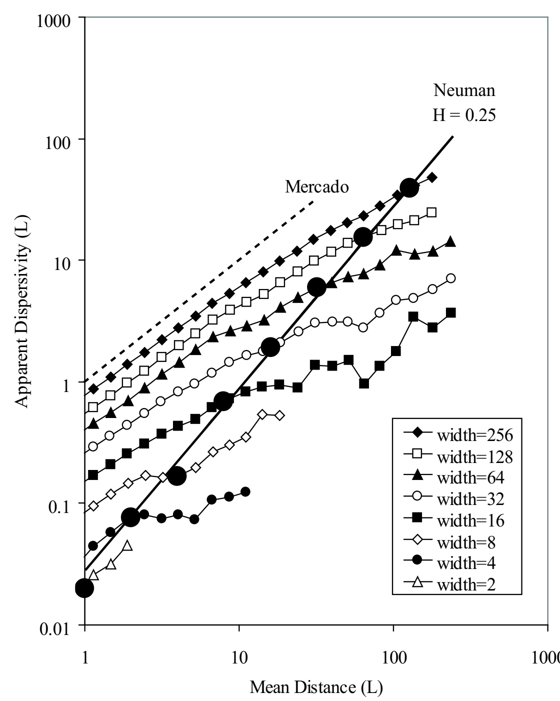

Figure 13. The effect of initial transverse plume dimensions on effective dispersion. Ensemble transport through purely isotropic fBm fields ($H = 0.25$) is investigated to best explore the validity of *Neuman's* [1990] universal scaling theory. When we "observe" effective dispersivity at a mean travel distance proportional to the initial plume width (black dots), we can see *Neuman's* apparent super-Mercado growth, although all individual and ensemble plume growth is limited to Mercado's linear growth.

In an elegant attempt to synthesize a universal dispersivity relationship, *Neuman* [1990] presented a plot of apparent longitudinal dispersivity versus scale of study from separate sites, demonstrating fractal behavior where $\alpha_L \propto \bar{X}^{1+2H}$, estimating $H = 0.25$ from the empirical fit to the data. Our simulations suggest that no single site will create super-Mercado growth, so the question remains—why do multiple plumes exhibit the "super-Mercado" growth? One possibility is the effect of initial plume size on longitudinal plume dispersion. Both transverse and longitudinal plume size have an effect on dispersion in fractal fields (Figure 13). In Figure 13 we have plotted effective dispersivity for plumes of varying initial width. Isotropic fBm fields were used ($H = 0.25$) to investigate the validity of *Neuman's* [1990] universal scaling theory. "Observations" of apparent dispersivity are made (large black dots) at mean travel distances proportional to the initial plume sizes. These imaginary "observations" are based on the conjecture that smaller initial plumes will not travel as far before natural attenuation or dilution will reduce them to undetectable levels. In short, larger initial plumes travel farther. In core and lab-scale tests this is unavoidable. Therefore, dispersivity measurements at small scales are likely a result of smaller initial plume sizes, and dispersivity measurements at larger travel distances are likely coming from larger initial plumes. When dispersivity is observed for various plume sizes when the mean travel distance is some proportion of the initial plume width, then a super-Mercado relation is observed (Figure 13). This effect of initial plume size on apparent dispersivity could give the appearance of a super-linear growth of apparent dispersivity as observed by *Welty and Gelhar* [1989], *Neuman* [1990] and *Gelhar et al.* [1992], although no individual or ensemble plume will actually exhibit such growth. Similar behavior was observed in anisotropic osfBm fields as well.

6. Discussion

A key assumption in the derivations by *Neuman* [1990] is that a fractal K-field produces a fractal velocity field. As a particle moves within a stream tube, it is assumed to always have a chance of encountering higher velocity zones, accelerating plume growth. However, if stream tubes are defined by a predominantly layered geometry, then they will have a fixed flux and cannot proportionately increase velocity through areas of higher K without violating conservation of mass requirements. On the other hand, our numerical results may be skewed due to the far-reaching influence of the artificial boundaries. These effects are typically assumed to be negligible [e.g. *Hassan et al.*, 1997]. To explore the possibility of significant boundary effects we conducted several ensemble simulations with sequentially smaller domain sizes. The results of these simulations matched the larger domain size simulations, suggesting that boundary effects are minimal.

Some analytic solutions have been proposed for the relation between transverse plume size and effective dispersion. *Dagan* [1994] emphasizes that any heterogeneities smaller than the size of the plume will contribute to dispersion, while larger scale heterogeneities will only affect uncertainty in the location of the plume. *Dagan* [1994] predicts that the effective dispersion will grow with l^2 for transverse plume dimension l. Some preliminary results indicate a weaker dependence of dispersion on transverse plume dimension. If we compare dispersivities for various plume sizes at the same travel distance in Figure 13 we observe a relationship closer to $\alpha \propto l^{0.5}$. At larger mean travel distance, the dispersivity data for smaller initial plumes becomes much more irregular (and is not shown), indicating that larger ensemble sets are needed for smaller plumes. Because the smaller initial ensemble plumes are very uncertain, it may be extremely difficult to predict the growth of small plumes in fractal hydraulic conductivity fields.

In all the simulations presented here we have neglected local dispersion, and modeled purely advective transport, in order to most closely match the analytic theories we wished to test. Nonetheless, the inclusion of significant local dispersion could appreciably change plume behavior. *Kapoor and Gelhar* [1994a, 1994b] and *Kapoor and Kitanidis* [1998] observed that local dispersion is the only process that leads to the destruction of concentration variance (or the spatial fluctuations in concentration). In our ensemble plumes we do not see a significant concentration variance (Figure 11). Furthermore, the plumes do not converge to a Gaussian, so that classical analytic theories about concentration variance may not apply. Further research involving the addition of local dispersion will be a valuable addition to the present research. In particular, local dispersion could have significant effects on the evolution of single-realization plumes, since particles will be less restricted to stream tubes.

Modeling real-world flow and transport problems with fractal fields is a difficult task given the extensive characterization necessary as well as the inherent uncertainty in the model. Similar to the present work, most research has attempted to characterize the average behavior across an ensemble of possible realizations [*Molz et al.*, 2004]. The ability to condition these fields given measured values of conductivity could vastly improve the practical utility of the model.

The simulations presented in this paper may also be generalized to 3-*d*. All the operator scaling properties as well as the mixing measure can easily be generalized to allow for another degree of freedom. The only significant issue will be computational capabilities, as an additional dimension adds to the computations many fold. It could prove useful to explore the use of block scale dispersivity, presented in *Liu and Molz* [1997b] to reduce the grid size in 3-*d*. *Liu and Molz* [1997b] found that fractal behavior could be modeled by using a coarser grid and representing smaller-scale heterogeneities by increased local-scale dispersivities. Our finding that the dispersivity is, to first order, approximately linear with mean distance would easily apply to the grid scale. Unfortunately, the transport is highly non-Gaussian so the practical limits of upscaling are unknown. This concept could be tested in 2-*d*, and if found to be an accurate alternative, could be applied to 3-*d* operator-scaling fields.

The mixing measures here assume some underlying connection between fractal behavior of depositional surface water systems (such as braided streams) and the underlying aquifers. This could be a possible (and simple) method for quantifying the statistical dependence structure of aquifers without the need for invasive characterization across a wide-range of scales. *Sapozhnikov and Foufoula-Georgiou* [1996] present a straightforward method for determining the fractal dimension of braided streams based on aerial photographs. Investigation into the relation between the surface and subsurface manifestations of fractal behavior could be extremely valuable.

7. Conclusions

- The growth of longitudinal dispersivity versus mean travel distance is limited to linear rates for both individual and ensemble plume growth in 2-*d* classical isotropic fBm fields. For smaller values of the Hurst coefficient the increase in apparent dispersivity falls off from linear growth at larger travel distances, but remains super-Fickian.
- The mixing measure $M(\theta)$ has a less significant impact on plume evolution when compared with the effects of variation in the transverse Hurst coefficient.
- Accurate predictions of flow and transport cannot be made based upon a single value of the longitudinal Hurst

coefficient due to the strong effects of the transverse Hurst coefficient as well as the radius of isotropy.

• The matrix stretching of the convolution kernel according to the anisotropy of the orthogonal Hurst coefficients has a very significant impact on the continuity of high- and low-K material within the aquifer. This stretching is heavily dependent on the radius of isotropy. Fields described by the exact same scaling matrix $\boldsymbol{Q}$ as well as mixing measure $M(\theta)$ may demonstrate different correlation structures based upon the chosen radius of isotropy.

• Because there is no fractal cutoff in our fBm fields, none of the individual plumes transition to Fickian or asymptotic growth, but always remain in a pre-asymptotic state.

• In all of the cases investigated (including individual and ensemble simulations) the plumes demonstrate nearly Mercado-type growth (apparent dispersivity proportional to mean travel distance). Results indicate that Mercado plume growth cannot be exceeded in 2-d operator-scaling fBm fields.

• In both fBm and osfBm fields, dispersivity of the plume centroids is limited to linear growth with mean centroid displacement. In fBm fields with large Hurst coefficients a significant portion of ensemble dispersivity is a result of dispersivity of individual plume centroids. For lower values of the Hurst coefficient, ensemble dispersivity is dominated by spreading of individual plumes, dispersivity of the centroids being much less important to the ensemble spreading.

• *Neuman's* [1990] observation of super-linear growth of apparent dispersivity with scale of study can be explained by the effect of initial plume size on transport. We hypothesize that initially larger plumes tend to persist longer and are typically observed at larger travel distances. If we "observe" apparent dispersivity at mean travel distances proportional to initial plume width, we can reproduce *Neuman's* [1990] super-linear growth, although all individual and ensemble plumes are limited to linear growth of apparent dispersivity.

8. Notation

α_L	–	longitudinal dispersivity $[L]$.
A	–	scalar order of fractional integration.
$B(d\boldsymbol{x})$	–	uncorrelated (white) Gaussian noise.
$B_H(\boldsymbol{x})$	–	isotropic fractional Brownian motion.
$B_\varphi(\boldsymbol{x})$	–	(operator) fractional random field.
d	–	number of dimensions.
fBm	–	fractional Brownian motion.
$G(x,h)$	–	fractional Gaussian noise, with increments h.
H	–	scalar Hurst coefficient.
$\boldsymbol{I}$	–	identity matrix.
$\boldsymbol{k}$	–	wave vector $[L^{-1}]$.
K	–	hydraulic conductivity $[LT^{-1}]$.
$M(\theta)$	–	measure of directional weight within $\varphi(\boldsymbol{x})$.
osfBm	–	operator-scaling fractional Brownian motion.
$\boldsymbol{Q}$	–	deviations from isotropy matrix.
R	–	radius of isotropy.
VAR(X)	–	variance of longitudinal particle travel distance X.
$\bar{X}$	–	mean particle longitudinal travel distance.
$\mu_{ln(K)}$	–	mean of the $ln(K)$ field.
$\sigma_{ln(K)}$	–	standard deviation of the $ln(K)$ field.
θ	–	unit vector on the $d-$dimensional radius of isotropy.
$\varphi(\boldsymbol{x})$	–	scaling (convolution) kernel.

Acknowledgments. The authors were supported by NSF grants DMS–0417972, DMS–0139943, DMS–0417869, DMS–0139927, DMS–0706440 and U.S.DOE Basic Energy Sciences grant DE-FG02-07ER15841. Any opinions, findings, and conclusions or recommendations expressed in this material are those of the authors and do not necessarily reflect the views of the National Science Foundation or the U.S. Department of Energy. The authors would also like to thank three anonymous reviews and Associate Editor Peter Kitanidis for very helpful feedback during the review process.

References

Ababou, R., and L. W. Gelhar, Self-similar randomness and spectral conditioning: Analysis of scale effects in subsurface hydrology, in Dynamics of Fluids in Hierarchical Porous Media, edited by J. H. Cushman, chap. XIV, pp. 393-428, Academic, San Diego, Calif., 1990.

Benson D. A., M. M. Meerschaert, B. Baeumer, H.-P. Scheffler, Aquifer operator scaling and the effect on solute mixing and dispersion, *Water Resour. Res.*, 42(1), 2006.

Berkowitz B., A. Cortis, M. Dentz, H. Scher, Modeling non-Fickian transport in geological formations as a continuous time random walk, *Rev. Geophys.*, 44, 2006.

Biermé, H., M. M. Meerscheart, and H. P. Scheffler, Operator scaling random fields. Stochastic Processes and their Applications, Vol. 117, pp. 312-332, 2007.

Bruining, J., D. van Batenburg, L. W. Lake, A. P. Yang, Flexible Spectral Methods for the Generation of Random Fields with Power-Law Semivariograms, *Mathematical Geology*, 29(6), 823-848, 1997.

Caccia, D.C., D. Percival, M.J. Cannon, G.M. Raymond, J.B. Bassingthwaighte, Analyzing exact fractal time series: evaluating dispersional analysis and rescaled range methods, *Physica A*, 246, 609-632, 1997.

Castle, J. W., F. J. Molz, S. Lu, and C. L. Dinwiddie, Sedimentology and fractal-based analysis of permeability data, John Henry member, Straight Cliffs formation (upper Cretaceous), Utah, U.S.A., *J. Sediment. Res.*, 74(2), 270-284, 2004.

Dagan, G., The significance of heterogeneity of evolving scales to transport in porous formations, *Water Resour. Res.*, 30(12), 3327-3336, 1994.

Deshpande, A., P. B. Flemings, and J. Huang, Quantifying lateral heterogeneities in fluvio-deltaic sediments using three-dimensional reflection seismic data: Offshore Gulf of Mexico, *J. Geophys. Res.*, 102(B7), 15,38515,402, 1997.

Di Federico, V., S. P. Neuman, Scaling of random fields by means of truncated power variograms and associated spectra, *Water Resour. Res.*, 33(5), 1075-1086, 1997.

Di Federico, V., S. P. Neuman, Flow in multiscale log conductivity fields with truncated power variograms, Water Resour. Res., 34(5), 975-988, 1998a.

Di Federico, V., and S. P. Neuman, Transport in multiscale log conductivity fields with truncated power variograms, *Water Resour. Res.*, 34(5), 963-974, 1998b.

Di Federico, V., S. P. Neuman, D. M. Tartakovsky, Anisotropy, lacunarity, and upscaled conductivity and its autocovariance in multiscale random fields with truncated power variograms, *Water Resour. Res.*, 35(10), 2891-2908, 1999.

Gelhar, L. W., and C. L. Axness, Three dimensional stochastic analysis of macrodispersion in aquifers, *Water Resour. Res.*, 19(1), 161-180, 1983.

Gelhar, L. W., C. Welty, and K. R. Rehfeldt, A critical review of data on field-scale dispersion in aquifers, *Water Resour. Res.* 28(7), 1955-1974, 1992.

Hassan, A. E., and J. H. Cushman, J. W. Delleur, Monte Carlo studies of flow and transport in fractal conductivity fields: Comparison with stochastic perturbation theory, *Water Resour. Res.*, 33(11), 2519-2534, 1997.

Herrick, M. G., D. A. Benson, M. M. Meerschaert, and K.R. McCall, Hydraulic conductivity, velocity, and the order of the fractional dispersion derivative in a highly heterogeneous system, *Water Resour. Res.*, 38(11), 2002.

Hewett, T. A., Fractal distributions of reservoir heterogeneity and their influence on fluid transport, Paper SPE 15386, presented at the 61st Annual Technical Conference, Soc. of Pet. Eng., New Orleans, La., 1986.

Kapoor, V., L. W. Gelhar, Transport in three-dimensionally heterogeneous aquifers 1. Dynamics of concentration fluctuations, *Water Resour. Res.*, 30(6), 1775-1788, 1994a.

Kapoor, V., L. W. Gelhar, Transport in three-dimensionally heterogeneous aquifers 2. Predictions and observations of concentration fluctuations, *Water Resour. Res.*, 30(6), 1789-1802, 1994b.

Kapoor, V., P. K. Kitanidis, Concentration fluctuations and dilution in aquifers, *Water Resour. Res.*, 34(5), 1181-1194, 1998.

Kemblowski, M. W., J.-C. Wen, Contaminant Spreading in Stratified Soils with Fractal Permeability Distributions, *Water Resour. Res.*, 29(2), 419-425, 1993.

LaBolle, E. M., G. E. Fogg, A. F. B. Tompson, Random-walk simulation of transport in heterogeneous porous media: Local mass-conservation problem and implementation methods, *Water Resour. Res.*, 32(3), 583-594, 1996.

Liu, H. H., and F. J. Molz, Multifractal analyses of hydraulic conductivity distributions, *Water Resour. Res.*, 33(11), 2483-2488, 1997a.

Liu, H. H., and F. J. Molz, Block scale dispersivity for heterogeneous porous media characterized by stochastic fractals, *Geophysics Research Letter*, 24(17), 2239-2242, 1997b.

Lu, S., F. Molz and H. H. Liu, An efficient, three-dimensional, anisotropic, fractional Brownian motion and truncated fractional Levy motion simulation algorithm based on successive random additions, *Computers and Geosciences*, 29(1), 15-25, 2003.

Mandelbrot, B. B., and J. R. Wallis, Noah, Joseph, and Operational Hydrology, *Water Resour. Res.*, 4(5), 909-918, 1968.

Mandelbrot, B. B., and J. R. Wallis, Computer Experiments with Fractional Gaussian Noises. Part 1, Averages and Variances, *Water Resour. Res.*, 5(1), 228-241, 1969a.

Mandelbrot, B. B., and J. R. Wallis, Robustness of the Rescaled Ranges R/S in the Measurement of Noncyclic Long Run Statistical Dependence, *Water Resour. Res.*, 5(5), 967-988, 1969b.

Mason, J. D., and Y. M. Xiao, Sample path properties of operator-self-similar Gaussian random fields, *Theory Probab. Appl.*, 46(1), 58-78, 2001.

Matheron, M., and G. de Marsily, Is transport in porous media always diffusive?, *Water Resour. Res.*, 16, 901-917, 1980.

Mercado, A., The spreading pattern of injected water in a permeability-stratified aquifer, *Int. Assoc. Sci. Hydrol. Publ.*, 72, 2336, 1967.

Molz, F. J., and G. K. Boman, A stochastic interpolation scheme in subsurface hydrology, *Water Resour. Res.*, 29, 37693774, 1993.

Molz, F. J., and G. K. Boman, Further evidence of fractal structure in hydraulic conductivity distributions, *Geophys. Res. Lett.*, 22, 25452548, 1995.

Molz, F. J., O. Güven, J. G. Melville, and C. Cardone, Hydraulic conductivity measurement at different scales and contaminant transport modeling, in *Dynamics of Fluids in Hierarchical Porous Formations*, edited by J. H. Cushman, pp. 37-59, Academic, San Diego, Calif., 1990.

Molz, F. J., H. H. Liu, and J. Szulga, Fractional Brownian motion and fractional Gaussian noise in subsurface hydrology: A review, presentation of fundamental properties, and extensions, *Water Resour. Res.*, 33(10), 2273-2286, 1997.

Molz, F.J., H. Rajaram and S. Lu, Stochastic fractal-based models in subsurface hydrology: Origins, applications, limitations and future research questions, *Reviews of geophysics*, 42, RG1002, 2004.

Neuman, S. P., Universal scaling of hydraulic conductivities and dispersivities in geologic media, *Water Resour. Res.*, 26(8), 1749-1758, 1990.

Neuman, S. P., On advective transport in fractal permeability and velocity fields, *Water Resour. Res.*, 31(6), 1455-1460, 1995.

Painter S., Mahinthakumar G., Prediction uncertainty for tracer migration in random heterogeneities with multifractal character, *Advances in Water Resources*, 23 (1), 49- 57(9), 1999.

Rajaram, H., and L. Gelhar, Plume-scale dependent dispersion in aquifers with a wide range of scales of heterogeneity, *Water Resour. Res.*, 31(10), 2469-2482, 1995.

Sapozhnikov, V., E. Foufoula-Georgiou, Self-affinity in braided rivers, *Water Resour. Res.*, 32(5), 1429-1440, 1996.

Tennekoon, L., M. C. Boufadel, D. Lavallee, and J. Weaver, Multifractal anisotropic scaling of the hydraulic conductivity, *Water Resour. Res.*, 39(7), 1193, 2003.

Welty, C., and L. W. Gelhar, Evaluation of longitudinal dispersivity from tracer test data, *Rep. 320*, Ralph M. Prsons Lab. for Water Resour. and Hydrodyn., Mass. Inst. of Technol., Cambridge., 1989.

Zhan, H., S. W. Wheatcraft, Macrodispersivity tensor for nonreactive solute transport in isotropic and anisotropic fractal porous media: Analytical solutions, *Water Resour. Res.*, 32(12), 3461-3474, 1996.

Nathan D. Monnig and David A. Benson, Department of Geology and Geological Sciences, Colorado School of Mines, 1500 Illinois St., Golden, CO, 80401, USA. (nmonnig@mines.edu, dbenson@mines.edu)

Mark M. Meerschaert, Department of Statistics and Probability, Michigan State University, A416 Wells Hall, East Lansing, MI 48824-1027, USA. (mcubed@stt.msu.edu)